

Nonlinear wind-up in a strained planar vortex

Charles Macaskill ^a, Andrew P. Bassom ^{b,*}, Andrew D. Gilbert ^b

^a School of Mathematics and Statistics, University of Sydney, NSW 2006, Australia

^b School of Mathematical Sciences, North Park Road, University of Exeter, Exeter, Devon EX4 4QE, UK

Received 5 January 2001; received in revised form 11 December 2001; accepted 16 January 2002

Abstract

The response of a Gaussian vortex to a strong external strain field is examined using two complementary numerical schemes. When the strain is weak previous calculations have shown that a rebound phenomenon is operative: after enstrophy is transferred from the mean to the azimuthal component by the straining there is a reversal during which a significant fraction of the enstrophy moves back from the azimuthal component to the mean. Concomitantly the perturbation vorticity undergoes spiral wind-up and develops a short-scale radial structure which becomes ever finer with time. We show that the rebound behaviour is suppressed by strong strain and that the intricate radial structure is simultaneously inhibited. We also give some indication of the modifications that are introduced when a strongly strained vortex is allowed to relax after the forcing field is switched off. © 2002 Éditions scientifiques et médicales Elsevier SAS. All rights reserved.

1. Introduction

Two-dimensional turbulent flows are typified by the behaviour that random small-scale initial conditions evolve to form coherent vortices which constitute the dominant feature of the flow field [1–3]. Vortices in high Reynolds number flow are frequently isolated in the sense that their separations are substantially greater than the length scales of the vortices themselves. On the larger scale the vortices move under their mutual interactions and at leading order are governed by the dynamics of a number of point vortices [4,5] while individual vortices can be regarded as approximately axisymmetric distributions of vorticity immersed in a time-dependent irrotational field generated by the other vortices [6]. In practice vortices placed in such strain fields are often observed to be quite robust both within turbulent and related geophysical flows, see for example Montgomery and Kallenbach [7].

Bassom and Gilbert [8] investigated the linear behaviour of strained planar vortices and used a combination of asymptotic and numerical methods to describe the way in which a large class of vortices can relax to axisymmetry. By this we mean that if a smooth two-dimensional vortex is perturbed then differential rotation tends to lead to wind-up of vorticity fluctuations to form a spiral. At infinite Reynolds number and within the linear approximation the vorticity distribution becomes axisymmetric in the weak sense that when the vorticity field is integrated against a smooth test function the result decays algebraically with time. However, it should be remarked that vortices do not inevitably relax to axisymmetry. Several works, including those by Dritschel [9,10], Kourmoutsakos [11] and Rossi et al. [12], have identified distributions that evolve to persistent, nonlinear, non-axisymmetric configurations. Indeed Rossi et al. conducted numerical experiments to explore the relaxation of Gaussian vortices subjected to perturbation and showed that for sufficiently strong disturbances the vortex evolves to a quasi-steady, rotating dipole; otherwise it settles back as an axisymmetric monopole.

Recent work has clarified when linear perturbations to stable vortices tend to axisymmetrize. For example, results obtained by Bernoff and Lingevitch [13] and Schecter et al. [14] confirm that Gaussian vortices do indeed axisymmetrize. While it is

* Correspondence and reprints.

E-mail address: drew@maths.ex.ac.uk (A.P. Bassom).

likely that this is also the case for general smooth, stable, non-compact vortices, we know of no formal proof of this (for partial results see Llewellyn Smith [15], Smith and Rosenbluth [16] and Briggs et al. [17]). On the other hand, compact vortices often permit undamped normal modes and so fail to axisymmetrize. If one superposes a ‘skirt’ of weak vorticity on a compact distribution, this causes damping of the normal mode because of the presence of a critical layer and then axisymmetrization occurs: the weaker the skirt the slower is the damping, as discussed by Schechter et al. [14], Briggs et al. [17], Le Dizès [18] and Balmforth et al. [19]. Put another way, the weaker the skirt then the longer the vortex will appear to behave like a compact vortex with some normal modes excited: however, ultimately, it will axisymmetrize. Nonlinear theory has been developed for the case of a compact vortex with a weak skirt of vorticity [19], but little is known in general about how nonlinearity affects the process of axisymmetrization for arbitrary distributions.

Computations described by Bassom and Gilbert [20] (hereafter referred to as BG99) were designed to investigate the nature of spiral wind-up and axisymmetrization within the weakly nonlinear regime. They examined three forms of time-dependent external field: an impulsive strain, an on-off step function and a continuous random input. Transfers of enstrophy between mean and azimuthal components were observed and a ‘rebound’ phenomenon noted. After enstrophy was transferred from the mean to azimuthal components by the external straining field, there was a subsequent reversal and much of the enstrophy moved back to the mean. The size of this reversal did depend on the type of the external strain applied but it was often a significant fraction of the original transfer from mean to azimuthal components. Long-time solutions developed by Lundgren [21] were used to account for the nature of the rebound behaviour and, in order to place this in context, results were compared with analogous passive scalar problems. This may be contrasted with Kida’s elliptical model [22,23] in which a vortex patch evolves inviscidly under its own flow field together with the external strain. The vorticity distribution remains elliptical in shape with the lengths and orientations of its principal axes governed by ordinary differential equations. The reversible ‘elastic’ behaviour of the Kida vortex is rather special and such vortices cannot axisymmetrize. We may contrast the behaviour of a Gaussian vortex in a weakly viscous flow, for which simulations show that azimuthal structure is generated and is then destroyed on the shear–diffuse time scale, see [5]. This is an irreversible process that reduces the enstrophy and appears to be typical of smooth, stable, non-compact vortices. While such a vortex can exhibit some features of the Kida model, the elastic behaviour is ultimately damped.

The objective of this paper is to extend the weakly nonlinear work of BG99 into the strongly nonlinear regime and thereby both investigate the limitations of their theory and explore the robustness of the various phenomena observed. Note that as the strain field is strengthened the process known as vortex stripping (Legras and Dritschel [24]) increasingly comes into play. Stripping occurs when the vortex loses vorticity from its periphery and what remains is a sharp edge. This behaviour can easily occur during close vortex encounters and the resulting sharp-edged vortices appear to be immune to the axisymmetrization which is very commonly observed for smoother distributions [10,24].

In realistic flows the leading non-trivial effect on an individual vortex due to its neighbours is that of strain and here we shall focus on the case of an external straining field with hyperbolic streamlines. This choice of distortion is motivated by the findings of BG99 which indicate both that it leads to significant rebound and that the perturbation enstrophy develops a very marked high wavenumber structure: the spatial frequency of this structure increases with time under a uniform straining field while the vortex relaxes to a steady strained state. In consequence there is the interesting picture of relaxation on larger spatial lengths while ever more intricate structure is being created on continuously shrinking scales through spiral wind-up in the relaxed state.

Our fully nonlinear investigation is inevitably numerical in character and our treatment is founded on two complementary methods – one based on pseudo-spectral techniques while the other uses ideas taken from a contour dynamics approach. Details of the two methods are postponed to Section 2.1 below after we have formulated the governing system of equations. The results of the numerical experiments are described in Section 3 and we conclude by offering some discussion in Section 4.

2. Governing equations and numerical techniques

Our derivation of the governing system is motivated by that of BG99 and begins by considering a vortex with vorticity ω and stream function ψ within an externally imposed irrotational flow ψ_{ext} . The evolution of the flow satisfies the dimensionless equations

$$\partial_t \omega = J(\psi + \psi_{\text{ext}}, \omega) + \text{Re}^{-1} \nabla^2 \omega, \quad (1)$$

$$\nabla^2 \psi = -\omega, \quad \nabla^2 \psi_{\text{ext}} = 0, \quad (2)$$

where

$$\nabla^2 \equiv \partial_r^2 + r^{-1} \partial_r + r^{-2} \partial_\theta^2, \quad J(a, b) \equiv r^{-1} (\partial_r a \partial_\theta b - \partial_\theta a \partial_r b), \quad (3)$$

written in terms of the usual polar co-ordinates (r, θ) . The Reynolds number Re is assumed to be very large, for although our principal theoretical interest lies in the inviscid limit $\text{Re} \rightarrow \infty$, numerical requirements mean that some diffusion has to be retained in the model.

The external stream function ψ_{ext} is assumed to be generated away from our chosen vortex by distant vortices or moving boundaries or some other device. Necessarily ψ_{ext} is harmonic and so has algebraic growth away from the vortex, but nearby it can be expanded as a sum of terms proportional to $r^n e^{in\theta} + \text{c.c.}$ for $n \geq 0$; wherever we use c.c. within a formula it denotes the complex conjugate of the preceding expression. The $n = 0$ term has no effect; the next, $n = 1$, only generates uniform flow which is not of interest here while the $n = 2$ term represents a straining of the vortex. Therefore, like BG99, we shall restrict our work to straining fields

$$\psi_{\text{ext}} = \varepsilon q(t) r^n e^{in\theta} + \text{c.c.}, \quad (4)$$

where $0 < \varepsilon \ll 1$ and the time-dependent strength of the mode and orientation of the axes are prescribed by the complex function $q(t)$. Note that there is no vorticity in the external stream function ψ_{ext} . Uniform vorticity, as in a shear flow, could be introduced, but to limit our parameter space we shall not do so. In fact uniform vorticity may be eliminated by moving to a rotating frame and changing the function $q(t)$.

All the subsequent calculations are conducted with $n = 2$ so that our forcing consists of a solitary azimuthal wavenumber – but this is the one which has the greatest effect on the ensuing dynamics. The governing system is expanded,

$$\omega = \omega_0(r, t) + \varepsilon(\omega_1(r, t) e^{in\theta} + \text{c.c.}) + \varepsilon^2(\omega_2(r, t) + \omega_{22}(r, t) e^{2in\theta} + \text{c.c.}) + \dots, \quad (5)$$

with an analogous expression for the stream function ψ . (Note that here we have retained the azimuthal wavenumber n in order to illustrate the overall structure of the equations even though it is implicit that $n = 2$ for the numerical results shown.) The terms ω_0 and ψ_0 represent the basic axisymmetric state of the vortex and, following BG99, we take the Gaussian form

$$\omega_0 = \frac{1}{4\pi} \exp(-r^2/4), \quad \psi_0 = -\frac{1}{2\pi} \left[\ln r + \int_r^\infty s^{-1} \exp(-s^2/4) ds \right], \quad (6)$$

which has unit circulation and period of rotation $16\pi^2$ at the centre.

In passing we remark that several previous works in this area have expressed strain rates in dimensionless form rather than the definition adopted here. Typically the strain is normalised by the peak vorticity of the vortex, and so, to facilitate comparison with this other work, it is helpful to introduce the relative strain parameter ε_r given by $\varepsilon_r = 16\pi\varepsilon$. The quantity ε_r is a useful measure of the magnitude of the strain: for instance it is known [22] that a relative strain of $|\varepsilon_r| > 0.15$ (or $|\varepsilon| \gtrsim 0.003$) is more than sufficient to completely destroy a Kida vortex.

On substituting expansions akin to (5) for ω and ψ into the system (1)–(3) we find that

$$\partial_t \omega_0 = \text{Re}^{-1} \Delta_0 \omega_0, \quad (7a)$$

$$\partial_t \omega_1 + in\alpha \omega_1 + in\beta(\psi_1 + qr^n) = \text{Re}^{-1} \Delta_1 \omega_1, \quad (7b)$$

$$\partial_t \omega_2 + inr^{-1} \partial_r [(\psi_1 + qr^n) \omega_1^*] + \text{c.c.} = \text{Re}^{-1} \Delta_0 \omega_2, \quad (7c)$$

$$\partial_t \omega_{22} + 2in(\alpha \omega_{22} + \beta \psi_{22}) - in^2 r^{-1} [\omega_1 (\partial_r \psi_1) - \psi_1 (\partial_r \omega_1) + nqr^{n-1} \omega_1] = \text{Re}^{-1} \Delta_2 \omega_{22} \quad (7d)$$

and

$$-\omega_0 = \Delta_0 \psi_0, \quad -\omega_1 = \Delta_1 \psi_1, \quad -\omega_2 = \Delta_0 \psi_2, \quad -\omega_{22} = \Delta_2 \psi_{22}, \quad (8)$$

where

$$\Delta_p \equiv \partial_r^2 + r^{-1} \partial_r - n^2 p^2 r^{-2}, \quad \alpha(r) \equiv -r^{-1} \partial_r \psi_0 \quad \text{and} \quad \beta(r) \equiv r^{-1} \partial_r \omega_0.$$

In the inviscid limit, enstrophy

$$E_\omega \equiv \frac{1}{2} \int \omega^2 d^2 \mathbf{r}, \quad (9)$$

is conserved and so, if initially the perturbation enstrophy is zero, then correct to $O(\varepsilon^2)$

$$e_\omega = \int_0^\infty (\omega_0 \omega_2 + |\omega_1|^2) 2\pi r dr = 0. \quad (10)$$

It is clear that within this expression we can identify two contributions: one comes from the mean terms in (5) while the other arises from the azimuthal component. If we label the two parts e_ω^{mean} and e_ω^{azi} so that

$$e_\omega^{\text{mean}} \equiv 2\pi \int_0^\infty r \omega_0 \omega_2 dr, \quad e_\omega^{\text{azi}} \equiv 2\pi \int_0^\infty r |\omega_1|^2 dr, \quad (11)$$

then (10) demonstrates that in the limit $\text{Re} \rightarrow \infty$ any increase (decrease) in e_{ω}^{azi} has to be balanced by an equal decrease (increase) in e_{ω}^{mean} .

2.1. Numerical methods

As one of the aims here is to investigate the domain of applicability of the weakly nonlinear equations (7) we need to be able to compare those results with some fully nonlinear simulations of (1)–(3). To tackle (7) we wrote this system as 24 coupled equations in r and t and solved these using a Keller-box method [25] taken from the NAG suite of routines. The equations were solved on a domain $0 \leq r \leq r_{\max}$, where the outer boundary r_{\max} was placed sufficiently far out so as to ensure that the necessary far-field decay had comfortably set in before it was reached. Standard regularity conditions were imposed at $r = 0$ and large- r asymptotes prescribed at $r = r_{\max}$ (see BG99 for details). For all the computations reported here the number of spatial points was fixed as 1001 with $r_{\max} = 10$ and $\text{Re} = 10^8$. Inclusion of some weak viscosity was necessary for numerical purposes but the choice made was such that the time scale of the viscous decay of mean and azimuthal fields is at least a factor of ten larger than the maximum times considered. We have ensured that viscosity has a negligible effect on the results described below and so our weakly nonlinear predictions can safely be taken as being truly inviscid.

One question that we wish to address concerns the size of the straining field beyond which weakly nonlinear theory ceases to provide an accurate description of the evolution of the flow. To this end, we developed a fully nonlinear pseudo-spectral code designed to solve the vorticity/stream function system (1)–(2) in a doubly-periodic box. This domain was chosen to be of size $16\pi \times 16\pi$ and so is considerably larger than the half-width ($r = 2$) of the initial Gaussian distribution (6). The box was sub-divided using 512 grid points in each direction so there were roughly 40–50 nodes spanning the central region occupied by the vortex. In order to stabilise the calculation the viscous diffusion term in (1) was replaced by the hyperviscous operator $-\nu_8 \nabla^8 \omega$. The parameter ν_8 was selected so that the effect of the term was to spatially filter at each time-step with the $1/e$ point of the filter at five-sixths of the maximum spatial frequency as determined from the grid spacing (for details see Macaskill and Bewick [26]). Finally, it should be noted that the doubly-periodic geometry introduces a weak background rotation equal to the vortex circulation divided by twice the area of the domain. Strictly this effect should be accounted for when describing the results but our region of integration was taken to be so large that in practice the corrections required could be safely ignored.

In order to validate our pseudo-spectral results an independent solution of the complete nonlinear problem was written using the CASL (Contour-Advective Semi-Lagrangian) algorithm on the same doubly-periodic domain. In the CASL philosophy at each time-step contours of vorticity are advected by the velocity field determined from a grid-based inversion of the Poisson equation (2). The pseudo-spectral solution of this equation requires an interpolation of the contours of vorticity onto a regular grid: thus the velocity field is only known to an accuracy determined by the rectangular grid used (here 512 square). However, it has been shown [27] that the vorticity is determined considerably more accurately than for the equivalent pseudo-spectral technique and that longer time-steps may be taken. For our purposes the most significant feature of the CASL approach is that it has extremely small artificial dissipation, introduced by the technique known as contour surgery, which involves breaking long thin filaments of vorticity and/or connecting thin but nearby filaments of equal vorticity value.

A key property to be emphasised in this work is that the dissipation within the CASL method is of completely different character to hyperviscous diffusion so that when equivalent results are obtained with the two nonlinear codes it is a positive indication that unwanted numerical dissipation is insignificant. To resolve the continuous variation of vorticity found across the Gaussian vortex twelve vorticity contours were introduced with the vorticity jumps selected so that equal contributions to the circulation were enclosed between each successive pair of contours.

3. Results

Almost all of the calculations described below were conducted using an external strain field of the form

$$\psi_{\text{ext}} = 2\varepsilon(x^2 - y^2); \quad (12)$$

in terms of (4) we have $q(t) = 1$ implying that ψ_{ext} is turned on at time $t = 0$ and is then constant indefinitely. The choice of initialisation is often a subject of some debate and it has been argued that an abrupt imposition of a straining flow is of less physical significance than a slower build-up which can be used to model vortices drifting far from a given vortex. The impulsive case tends to induce large non-axisymmetric disturbances while the more gradual problem gives rise to a more benign response as discussed in [24]. Very recent studies by Legras et al. [28] suggest that a vortex within a slowly growing strain field evolves through a sequence of approximate equilibrium states until at some critical strain value it suddenly breaks. In this paper we concentrate on the impulsive problem, although we shall make a brief comparison with a slower build-up of strain in Section 4.

At first glance it is unclear how the strain field should be imposed within our doubly periodic computational domain. The strain field as defined above is not periodic, but rather undergoes a jump at the boundary. In principle this leads to an

inconsistency, in that the vorticity may then also jump there. However, as the vorticity is very close to zero at the boundary of the domain, any residual jump is of no consequence. It is possible to apply an exponential filter to the strain field near the boundary in order to guarantee periodicity, but this refinement was not required here.

BG99 showed that when the Gaussian vortex (6) is distorted by a field like (12) there is a strong transfer of enstrophy to the azimuthal component of perturbation enstrophy e_ω^{azi} followed by an oscillatory relaxation of e_ω^{azi} back to a final non-zero level; moreover, this effect was considerably more marked for the strained vortex than for the parallel problem in which a passive scalar is advected within a straining flow. It is of interest to determine the robustness of this behaviour as the magnitude of the strain is enhanced.

3.1. Steady strain: small ε

In Fig. 1 we present the time evolution of the perturbation enstrophy when the amplitude parameter $\varepsilon = 5 \times 10^{-4}$ ($\varepsilon_r \simeq 0.025$). The total first azimuthal component e_ω^{azi} with $n = 2$ was computed in two ways. First, the Keller-box method was used to compute the $\mathcal{O}(\varepsilon^2)$ part of e_ω^{azi} (see (11)) using the strategy adopted by BG99. For comparison purposes the pseudo-spectral technique was also implemented and Fig. 1 shows that there is acceptable agreement between the two approaches. We should note that the turnover time of the Gaussian vortex (6) is $T = 16\pi^2 \approx 158$, based on its angular velocity at the centre, and increases outwards with, for example $T = 16\pi^2(1 - e^{-1})^{-1} \simeq 250$ at a radius $r = 2$. Thus the run in Fig. 1 up to $t = 800$ represents roughly five turnover times.

Figure 1 illustrates the presence of the rebound effect – it appears that the initial transfer of enstrophy from mean to azimuthal components takes e_ω^{azi} up to about 1600 but about half of this is subsequently lost through the reverse exchange back to the mean. This value, e_ω^{mean} , was also computed using both the Keller-box and the pseudo-spectral methodologies although it is important to emphasise that throughout this paper the latter technique uncovered the *total* axisymmetric enstrophy, that is *not* just the $\mathcal{O}(\varepsilon^2)$ part e_ω^{mean} (11). The pseudo-spectral code also enabled us to calculate the total perturbation enstrophy, which should be identically zero for all times. Figure 1 demonstrates that the weakly nonlinear approximation is clearly quite accurate at this relatively low level of strain and that our code is well behaved for times up to about $t = 600$. After this the total enstrophy shows signs of no longer being conserved according to the pseudo-spectral routine – monitoring of the perturbation vorticity field indicates that this break down is due to the first filament of vorticity reaching the boundary of the computational region.

Further evidence as to the relative performances of the two methods is given in Fig. 2 which depicts the radial distributions of the fundamental $e^{2i\theta}$ mode ω_1 and mean flow correction ω_2 (see (5)) at two selected times. The structures were determined from the pseudo-spectral results by interpolating the vorticity from the Cartesian grid onto a radial grid and then taking discrete Fourier transforms to recover the individual azimuthal modes. There are relatively minor differences between the two calculations but the gross features are consistent. This suggests that at this low level of strain the weakly nonlinear analysis captures the essential physics of the dynamics. Equivalently, the additional modes included in the pseudo-spectral code are so small as to be, at most, of only very marginal importance.

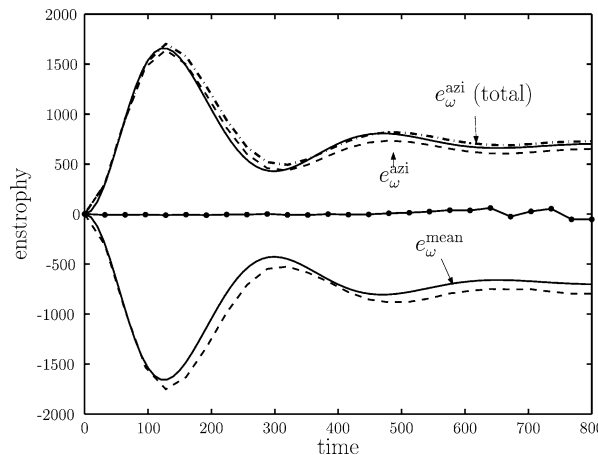


Fig. 1. Results for the evolution of enstrophy using the external strain (12) with $\varepsilon = 5 \times 10^{-4}$. The forms of e_ω^{azi} and e_ω^{mean} (see (11)) according to the weakly nonlinear approach of BG99 are shown with solid lines while the corresponding pseudo-spectral results are indicated dashed. The total perturbation enstrophy for the pseudo-spectral model (which should be zero) is denoted by the bold line distinguished with the bullets. Last, the full non-axisymmetric perturbation enstrophy from the pseudo-spectral method (that is including *all* the non-axisymmetric modes and not just the weakly nonlinear contributions) is designated by the dot-dash curve.

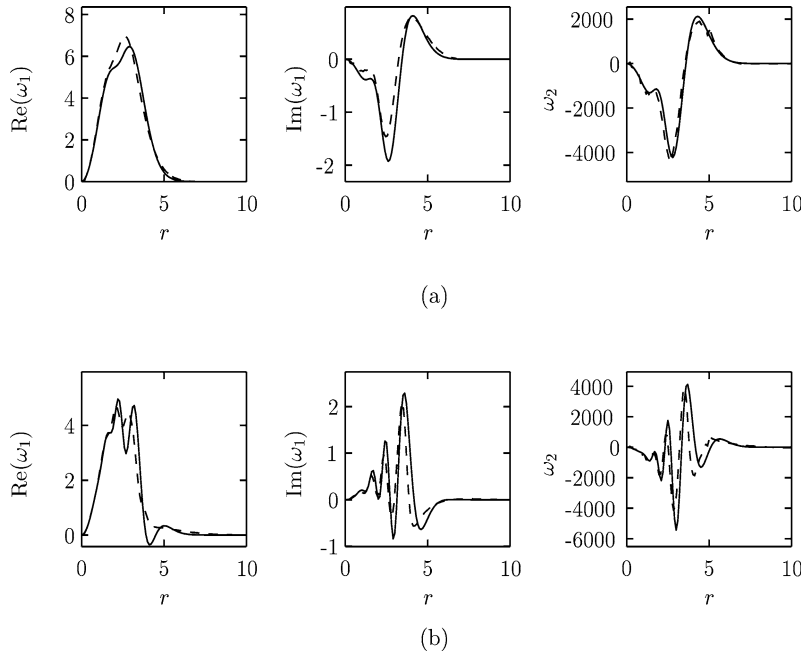


Fig. 2. (a) The radial structure of the $e^{2i\theta}$ mode ω_1 (first two frames) and the mean correction ω_2 (last frame) for $\varepsilon = 5 \times 10^{-4}$ and time $t = 160$. The solid lines denote the results using the Keller-box routine on the weakly nonlinear system (7) while the pseudo-spectral results are given by the dashed curves. (b) As (a) except for time $t = 384$.

We remark on the oscillations in the radial structure which increase in frequency as time advances corresponding to the fine-grained structures identified by BG99. These radial oscillations correspond to spiral perturbations in the vorticity once the angular dependence is accounted for, and will be destroyed on an $O(\text{Re}^{1/3})$ shear-diffuse timescale [5]. At this time the non-axisymmetric component ω_1 will relax to a steady solution of (7b), which is an inviscid perturbation to a Gaussian vortex, forced by strain. These solutions have been analysed by Jiménez et al. [29] and a comparison between these steady states and our weakly nonlinear simulations is given in Fig. 6 of [20]. Indeed at the moderate time $t = 384$ shown in Fig. 2(b) the solution for the real part of ω_1 is already close to the solution in [29]. Note that the theory of [29] applies to *any* initial vortex and gives its structure at long times of $O(\text{Re})$, with a Gaussian axisymmetric component; the theory applies to our configuration at rather earlier times simply because we chose to start with a Gaussian initial condition.

It turns out that the rebound phenomenon is closely related to the damping of quasi-modes on the Gaussian vortex. The study of [14] predicted a decay rate of quasi-modes of $0.079/4\pi \simeq 0.0063$ in our units, while simulations performed in [8] identified three important time regimes during the evolution of the vortex. The first of these regimes, corresponding to relatively early times in the rebound process (see [8], Fig. 1, regime A), consists of a decay which matches the damping rate obtained in [14].

3.2. Steady strain: moderate ε

The results described thus far give us confidence that the weakly nonlinear system is an accurate approximation for the full forms at least for small strains. This is of no surprise of course, but our next concern is how the situation changes as the amplitude ε is increased. Figure 3 summarizes the important features of the development for the two values $\varepsilon = 0.001$ ($\varepsilon_r \simeq 0.0503$) and $\varepsilon = 0.002$ ($\varepsilon_r \simeq 0.101$). (In both cases the results are shown for times prior to the first filament of vorticity reaching the boundary.) Let us take the smaller ε first – see Fig. 3(a). The situation here is remarkably similar to that shown in Fig. 1. There is good agreement between the weakly nonlinear and pseudo-spectral predictions but already we can see the reduction in the rebound phenomenon compared with Fig. 1. Note that BG99 showed that for other forms of input strain the rebound can be somewhat greater – indeed for an impulsive external strain the rebound is about three-quarters of the peak values. However, it should be remarked that a situation for which $q(t) = 0$ (see (4)) in the final state is somewhat different in character to one for which $q(t) \neq 0$ eventually. In the former case simulations indicate that axisymmetrization takes place (for small enough ε , here up to 0.001) while in the latter situation relaxation to a non-axisymmetric strained state occurs.

By the point $\varepsilon = 0.002$, see Fig. 3(b), some significant changes have taken place. The strength of the rebound is noticeably reduced and, importantly, weakly nonlinear theory no longer provides an accurate description of the full problem. Two features

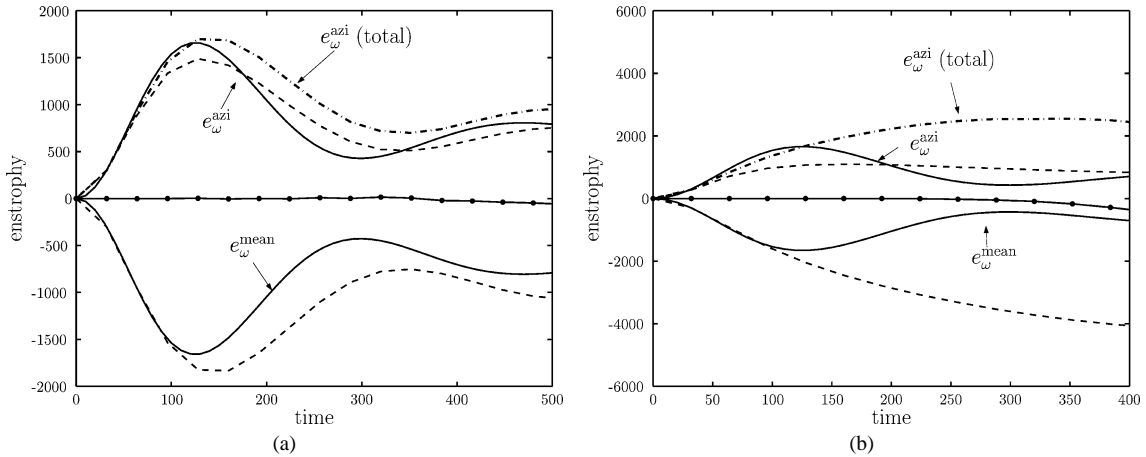


Fig. 3. As Fig. 1 except the strain field is now enhanced. (a) $\varepsilon = 0.001$, (b) $\varepsilon = 0.002$.

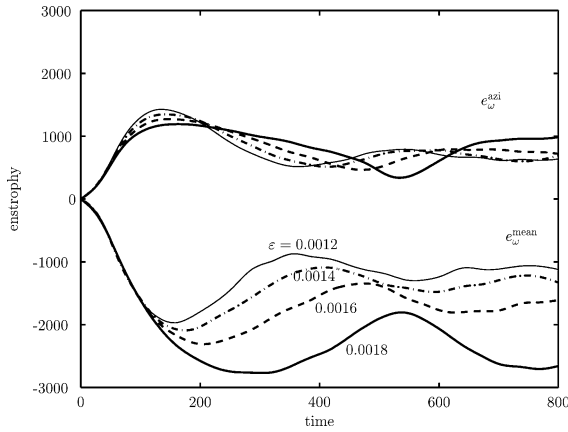


Fig. 4. Pseudo-spectral results for the evolution of enstrophy using the external strain (12) with $\varepsilon = 0.0012$ – 0.0018 in steps of 0.0002.

alert us to this: first the weakly nonlinear and pseudo-spectral results exhibit large differences beyond time $t \approx 100$ and, second, the dot-dashed line shows that a high proportion of the total non-axisymmetric perturbation enstrophy is contained in the higher azimuthal wavenumber modes. Weakly nonlinear theory is obviously incapable of capturing this behaviour and has comprehensively broken down.

In Fig. 4 we provide information on the evolution of the flow behaviour as ε changes from 0.001 to 0.002. It is apparent how the strength of the rebound behaviour diminishes with ε and that the minimum value of e_ω^{mean} is delayed to later and later times. Notice also that the proportion of azimuthal enstrophy contained in the higher harmonics grows with ε , which confirms our earlier comment that for strains ε much beyond 0.001 weakly nonlinear theory is untenable. We reiterate that although at first sight $\varepsilon = 0.002$ appears a disappointingly small value for weakly nonlinear theory to break down, $\varepsilon \approx 0.003$ would be sufficient for the strain to virtually destroy a Kida vortex. Moreover, Legras et al. [28] have shown recently that the strain needed to tear apart a distributed vortex is about three-quarters of that required to destroy a vortex patch. Thus $\varepsilon = 0.002$ does not represent particularly small values of strain in these terms. In addition, in experiments relating to response to a step input, BG99 pointed out that the weakly nonlinear formulation is only guaranteed to be good for times satisfying $\varepsilon t \ll 1$. Given the long turnover time of our basic vortex state it is essential that we integrate for several hundred time units to uncover the full evolution of the perturbation quantities and therefore it is unsurprising that there is an apparently tight restriction on ε before weakly nonlinear theory breaks down. Indeed the results in Figs. 3 and 4 only show significant deviations between the two computation methods when εt exceeds about 0.2 in accordance with the remarks in BG99.

Next we examine the detailed radial structure of the first two azimuthal modes. Figure 5 illustrates the forms of ω_1 and ω_2 for strain amplitude $\varepsilon = 0.001$ at the three times $t = 64, 192$ and 384 . There are systematic deviations between the weakly nonlinear and pseudo-spectral results – deviations which increase with time in line with our earlier comment that weakly nonlinear results are likely to become of ever decreasing usefulness as time advances. At the earliest time there is little difference between the

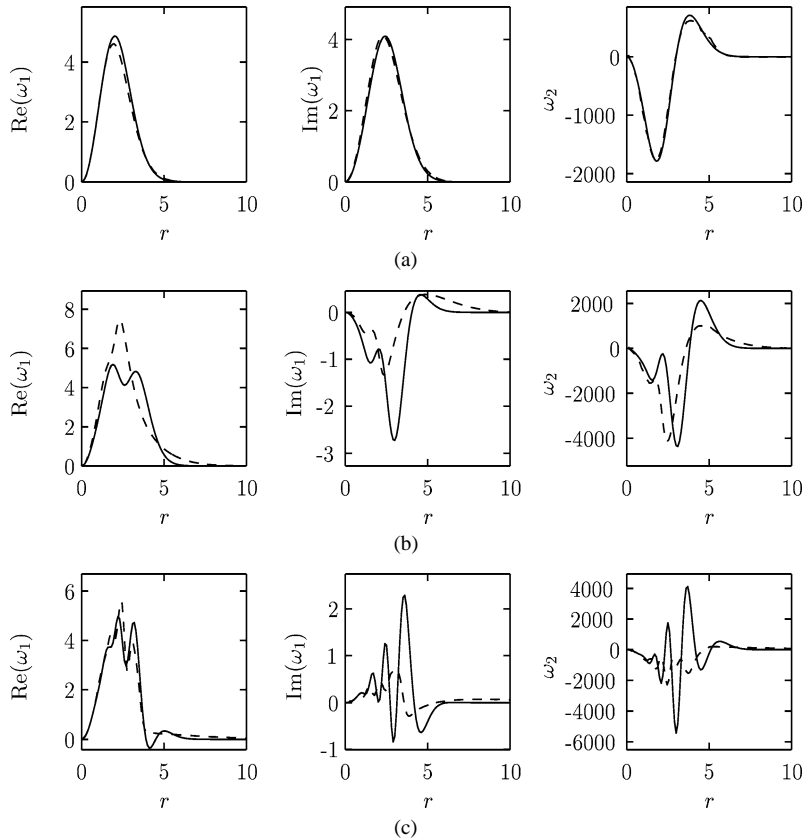


Fig. 5. Radial structure of ω_1 and ω_2 for external strain magnitude $\varepsilon = 0.001$. The solid lines denote the results using the Keller-box routine on the weakly nonlinear system while the pseudo-spectral results are given by the dashed curves. (a) $t = 64$, (b) $t = 192$ and (c) $t = 384$.

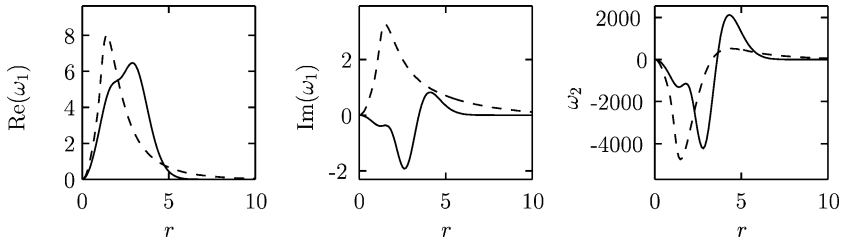


Fig. 6. As Fig. 5 except that $\varepsilon = 0.002$ and only time $t = 160$ is shown.

two forms of solution but as time passes so the picture changes. By $t = 384$, although there is some similarity in the structures of ω_1 , the mean flow corrections ω_2 predicted by the Keller-box and pseudo-spectral methods bear virtually no resemblance. The pseudo-spectral forms of these quantities appear to be both strongly suppressed in magnitude and to have lost some of the rapid oscillations predicted by BG99. These trends continue to be evident in Fig. 6, which is concerned with the case $\varepsilon = 0.002$. By this stage there appears to be little evidence of radial oscillatory behaviour in the pseudo-spectral results.

Scrutiny of Fig. 3(a) shows that by time $t = 400$ there are signs of hyperviscous dissipation as indicated by the departure of the total perturbation enstrophy from zero. It is possible that the loss of radial structure in the pseudo-spectral findings of Figs. 5 and 6 at large amplitude strains could be due to this same numerical dissipation. In order to ascertain whether this is the case, we sought further information concerning the fully nonlinear modes using the CASL [27] code with $\varepsilon = 0.002$. The final output is generated on a 512 square grid although the accuracy with which the vorticity contours are advected corresponds to a much higher resolution calculation. It was found that the radial structure of the azimuthal modes was essentially identical to that computed by the pseudo-spectral code while the total perturbation enstrophy was better conserved due partly to the very different numerical dissipation involved as introduced by the contour surgery technique (cf. the CASL results shown in Fig. 7

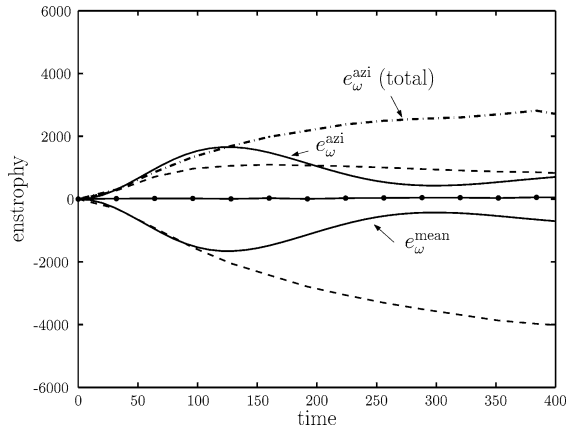


Fig. 7. As Fig. 1 except that the strain field amplitude $\varepsilon = 0.002$ and the dashed and dot-dash curves are computed using the CASL method.

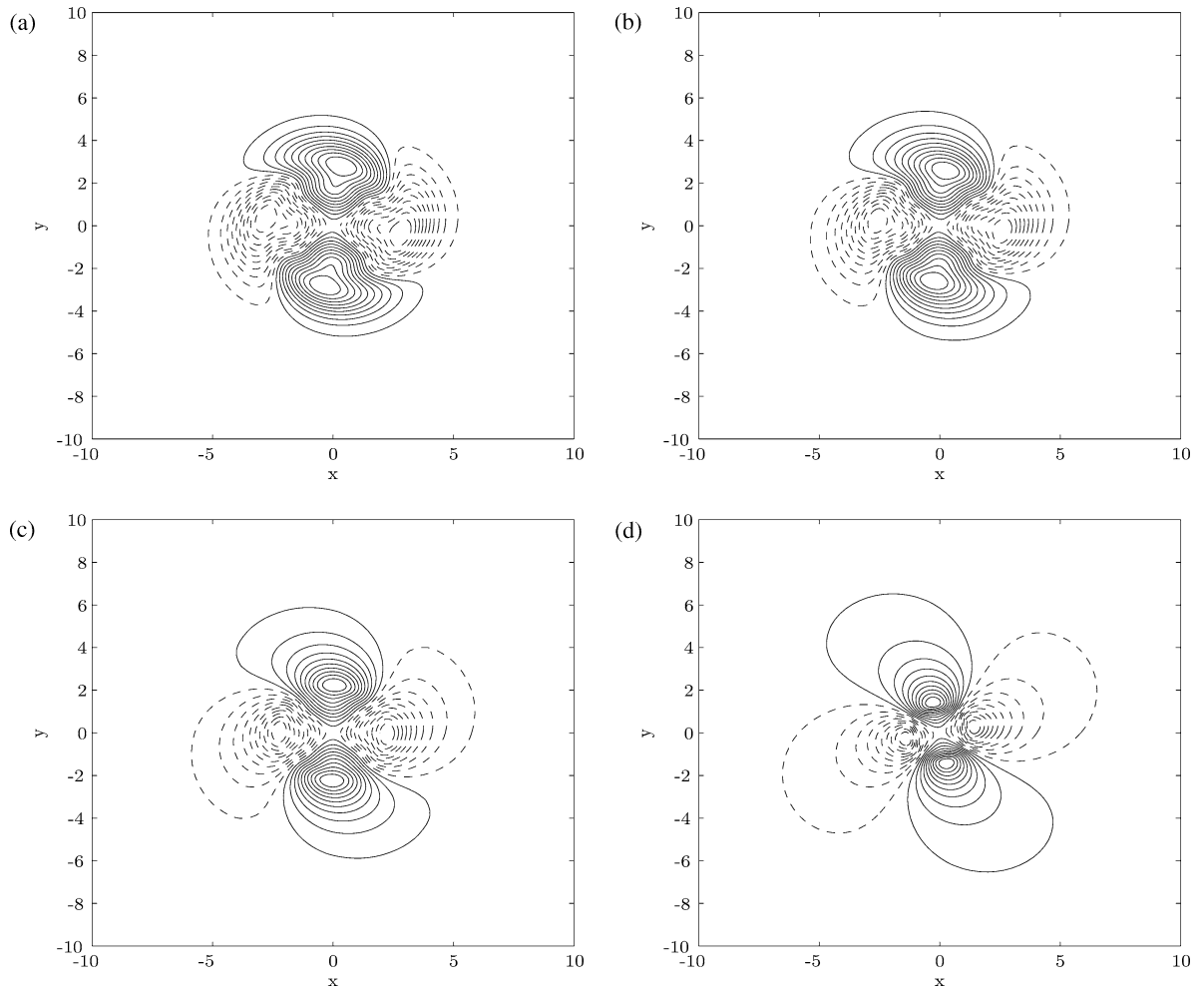


Fig. 8. Contours of the first azimuthal mode $\text{Re}(\omega_1 e^{2i\theta})$ at time $t = 160$. In (a) is shown the structure according to weakly nonlinear theory while (b)–(d) give the pseudo-spectral results for $\varepsilon = 5 \times 10^{-4}$, 0.001 and 0.002, respectively. In each case there are ten equally spaced contour intervals from zero to the maximum perturbation value (shown with solid lines) with a similar representation from zero to the most negative value (shown dashed).

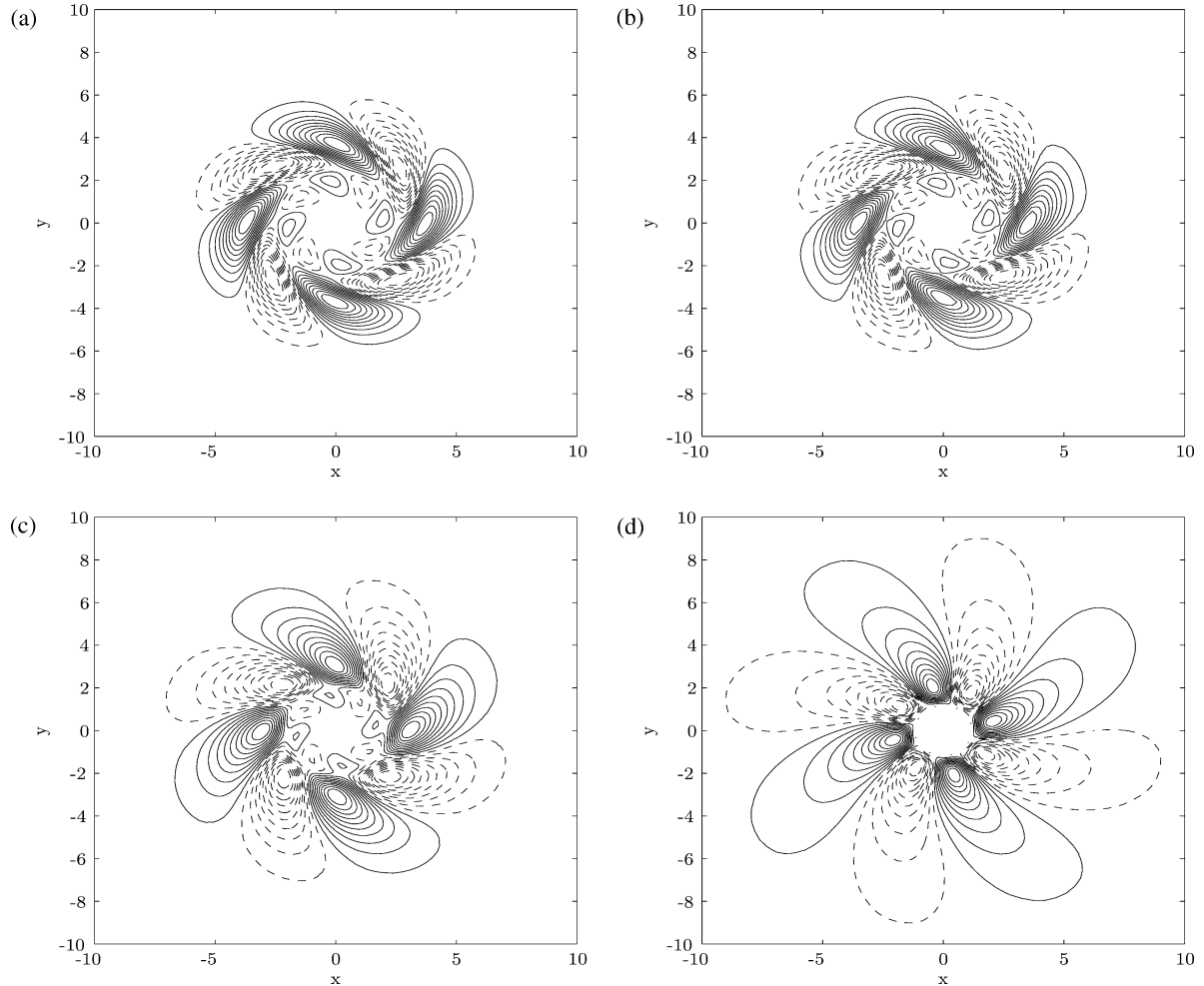


Fig. 9. As Fig. 8 except results are now for the second azimuthal mode $\text{Re}(\omega_{22} e^{4i\theta})$.

with their pseudo-spectral counterparts illustrated in Fig. 3(b)). This gives confidence that our fully nonlinear predictions are reliable.

Now we turn to consider the spatial distribution of the perturbation vorticity. Figures 8 and 9 illustrate the forms of $\text{Re}(\omega_1 e^{2i\theta})$ and $\text{Re}(\omega_2 e^{4i\theta})$ for a selection of strain magnitudes and the time $t = 160$. In other words, these plots show the actual vorticity distributions corresponding to the first two modes. Figure 8(a) indicates the weakly nonlinear predictions arising from BG99 while (b)–(d) demonstrate the changes that are induced as the external strain is gradually increased. It is evident that the fundamental azimuthal mode stays localized and that there is a tendency for the weak spiralling feature to be lost with enhanced strain. The corresponding results for the second mode, see Fig. 9, shows this effect with much more clarity. The well-defined spirals present in the weak $\varepsilon = 5 \times 10^{-4}$ case are virtually completely extinguished once $\varepsilon = 0.002$ and there is a tendency for this mode to spread from the centre of the vortex. We also see the explanation of the results presented in Fig. 6 which suggested that high frequency radial structure is lost as ε grows – this is a consequence of the damping of the spiral form which exists in the linearized and weakly nonlinear versions of the problem. Indeed, under the auspices of weakly nonlinear theory, at later times the spirals become ever more tightly wound as the spatial oscillations in radius increase in frequency. However, once the strain field becomes significant this behaviour disappears.

3.3. Unsteady strain

Last, we consider briefly the fate of the vortex should the constant external straining field be shut off at some time. To do this we conducted an experiment with the largest strain used, $\varepsilon = 0.002$, in which the straining was removed at $t = 200$, some time before any filaments reach the boundary of our computational domain. The weakly nonlinear predictions are compared

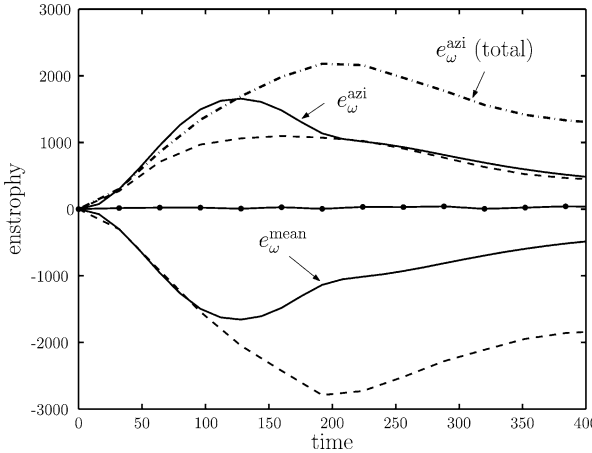


Fig. 10. The perturbation enstrophy as a function of time as in Fig. 7 except that the external strain is switched off at time $t = 200$.

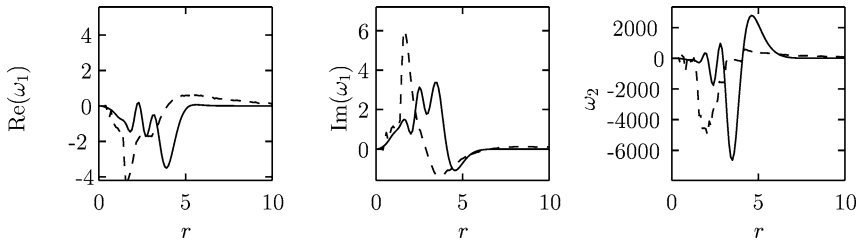


Fig. 11. Radial structure of ω_1 and ω_2 at time $t = 384$ for an external strain of magnitude $\varepsilon = 0.002$ which is removed at time $t = 200$. The solid lines denote the results using the Keller-box routine on the weakly nonlinear system while the CASL results are shown by the dashed curves.

with the results of a CASL calculation in Fig. 10. The integrated perturbation enstrophy for the first mode, e_ω^{azi} , shows quite good agreement with the weakly nonlinear theory although the latter tends to over-estimate the decay of the mode. Of course there are wide discrepancies in the forms of e_ω^{mean} for times much later than $t = 100$ (a point made with reference to Fig. 3(b) previously) and the CASL code confirms that the higher modes contain very significant proportions of the total azimuthal perturbation enstrophy. In fact, the relatively good agreement in the forms of e_ω^{azi} appears to be to some extent fortuitous; this is reflected by the results of Fig. 11 which shows the comparisons of the radial structures of the modes at time $t = 384$. This is long after the external straining has been removed and it is obvious that there is a significant memory effect at work here with the enhanced oscillations still present in the weakly nonlinear results. Another view of the development of the vorticity is provided in Fig. 12 which shows a time-sequence for the non-axisymmetric component of the perturbation enstrophy (if the full perturbation enstrophy were plotted then an extra Gaussian blob of negative vorticity would have to be superposed). At early times we see how the imposed strain leads to the formation of a filament of vorticity which is indicative of the onset of vortex stripping: after the strain is switched off at time $t = 200$ the natural rotation of the vortex leads to the winding-up of this filament. It should be emphasised that this behaviour is somewhat different from the ideas of vortex axisymmetrization and the creation of fine radial structure. In this event the whole vortex essentially becomes axisymmetric while in the wind-up illustrated in Fig. 12 although the filament structure certainly does tend to axisymmetry, the central portion of the vortex retains its distinctive $n = 2$ type form reminiscent of the triple pole structures obtained by Rossi et al. [12].

It is of interest to know whether the final non-axisymmetric state occurs irrespective of the size of the applied strain. To provide some insight into this aspect we explored the evolution of the vortex when subjected to various strengths of strain all shut off at time $t = 200$. Our results are summarised in Fig. 13 which illustrates the form of the quantity $|Q(t)|$ where

$$Q = m_{xx} - m_{yy} - 2im_{xy} \quad \text{and} \quad \{m_{xx}, m_{xy}, m_{yy}\} = \int \int \{x^2 \omega(r, \theta, t), xy \omega(r, \theta, t), y^2 \omega(r, \theta, t)\} dx dy,$$

where the integral is taken over the 16π -square domain and ω is now the perturbation vorticity divided by ε . The function $Q(t)$ was introduced by Rossi et al. [12] and it is known that in the far-field $\psi \propto Q(t)r^{-n}$ (see [8]). The upshot is that if the perturbation vorticity is to become axisymmetric as $t \rightarrow \infty$ then $Q(t) \rightarrow 0$ in this limit. It is clear from Fig. 13 that this indeed occurs for the weakly nonlinear calculations given by BG99. However, the finite amplitude extension counterpart converges non-

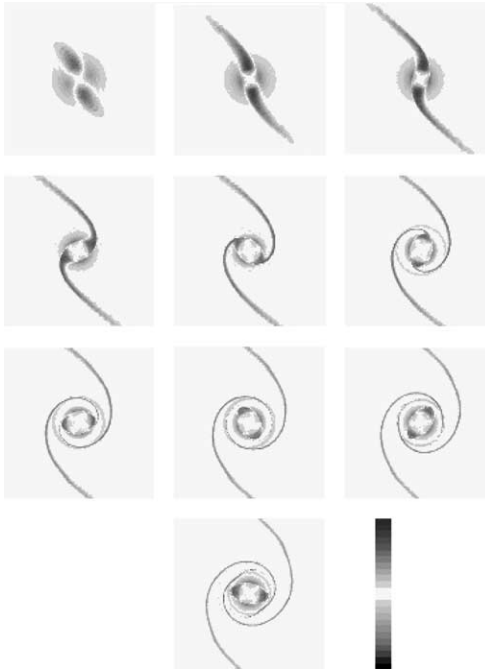


Fig. 12. Evolution of the non-axisymmetric component of perturbation enstrophy when the vortex is subjected to a strain field with $\varepsilon = 0.002$ that is switched off at $t = 200$. The panels show the development through times $t = 80, 160, 240, \dots$

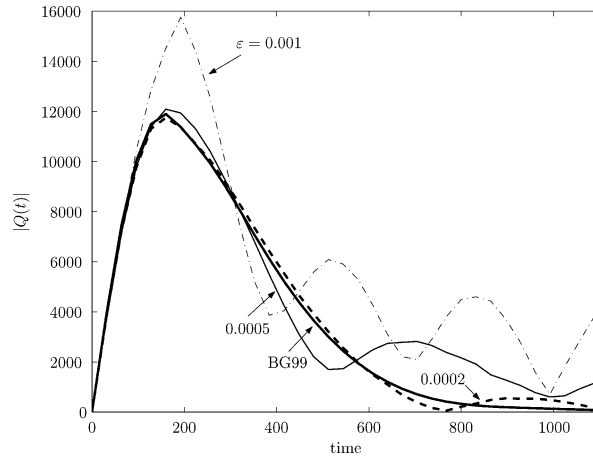


Fig. 13. Evolution of $|Q(t)|$ when the vortex is subject to a strain field that is switched off at $t = 200$, where the magnitude of the strain ε has the values 0.0002, 0.0005 and 0.001. Comparison is made with the weakly nonlinear results of BG99 (thick solid curve).

uniformly in that at large t the corresponding $|Q(t)|$ oscillates within a slowly decaying envelope. Unsurprisingly the magnitude of the oscillation decreases as ε is reduced but there is no evidence of a critical strain level above which axisymmetrization completely disappears, but rather a continuous increase in the magnitude of oscillation of $|Q(t)|$ (and accordingly the level of non-axisymmetry) at any given time as ε is increased. These conclusions must be taken to be somewhat tentative as much longer integration times are really necessary to determine whether $Q(t)$ properly vanishes as $t \rightarrow \infty$ rather than just saturating at some low level.

The angular velocity itself can also be estimated from the second order moments, using the algorithm described by Rossi et al. [12]. There are significant fluctuations in these measurements (in phase with the oscillations seen in $|Q(t)|$ in Fig. 13). For $\varepsilon = 5 \times 10^{-4}$ we find that the maximum angular velocity is about 0.008, which is in general agreement with both the numerical results of Rossi et al. [12] for different initial conditions, and with the theoretical study of Le Dizès [18]. As ε is increased the

level of fluctuations increases which makes the maximum angular velocity more difficult to measure, but the overall trend is that the angular velocity falls as the strain is enhanced.

4. Discussion

We have used numerical methods to investigate the processes of axisymmetrization and spiral wind-up which occur when a strong straining field is applied to a planar vortex. It is of importance to appreciate how the various computational approaches complement and contrast each other. In some cases two methods gave virtually identical results while in others there were significant differences. Although this might at first seem troublesome, in fact the divergence merely gives an indication as to when the borders of the various parameter ranges of validity are being breached. For example, the comparison of the Keller-box results and the pseudo-spectral findings illustrate that weakly nonlinear theory is useful at relatively low strain rates, but a point comes beyond which it ceases to have any validity. It is at this stage that the observed phenomena become truly fully nonlinear in character and reliable results can only be obtained under a completely nonlinear study. These cases were investigated by the pseudo-spectral and CASL codes and the fact that good agreement could be obtained despite the very different ways in which dissipation is treated lends further credence to our results.

In this study we have concentrated on the problem for which the external strain field is imposed impulsively. In many applications it might be expected that the strain builds up more slowly and to assess this aspect we repeated some of our calculations with a time-dependent strain field. Specifically, we chose $\varepsilon = \varepsilon(t) = \varepsilon_0 \tanh(\alpha t/20)$ with ε_0 and α prescribed constants and the corresponding evolution of enstrophy is summarized in Fig. 14. In this figure α takes a range of values from 0.1 (which corresponds to the case that about 96% of the maximum strain is achieved by time $t \approx 200$) through to the instantaneous switch-on case ($\alpha \rightarrow \infty$). We observe that the rebound phenomenon is quite robust so long as the maximum strain imposed is reached at or near the time at which the peak in e_ω^{azi} (Eq. (11)) is seen in the instantaneous problem. As an example, for $\alpha = 0.2$ we see that the rebound is still very evident although it is significantly damped. It appears that the rebound phenomenon can be effectively suppressed by allowing a sufficiently slow build-up of the straining field.

Of course, the primary interest for this study is to describe the way the picture painted by BG99 for the weakly nonlinear problem is modified as the intensity of the strain is increased. It should be emphasised that our calculations have confirmed the conclusions reached by BG99 that for weak strain there is a significant rebound phenomenon at work, the perturbation enstrophy develops a distinctive high-wavenumber structure whose spatial frequency grows with time and meanwhile the vortex relaxes to a steady strained state. As the strain is increased these major characteristics become much less marked – while the rebound behaviour is moderately robust it does eventually all but disappear at significant strain rates. In concert, the rapid radial oscillations are virtually extinguished although if the forcing is switched off there is some tendency for the radial structure to return. Our study forms a foundation for consideration of more intricate cases such as the extension to relaxing strained vortices within high Reynolds number shear flows [29].

The different behaviours obtained above for weak and strong strain have analogies with recent studies of perturbed vortices for which the results also depend on the strength of the strain. In the case of weak forcing smooth vortices tend to axisymmetrize after the strain is switched off; however, for stronger strains the vortex can bifurcate to a non-axisymmetric, steadily rotating state [9–12] and the process of spiral wind-up is arrested. In our calculation summarised by Fig. 12 vorticity was stripped from

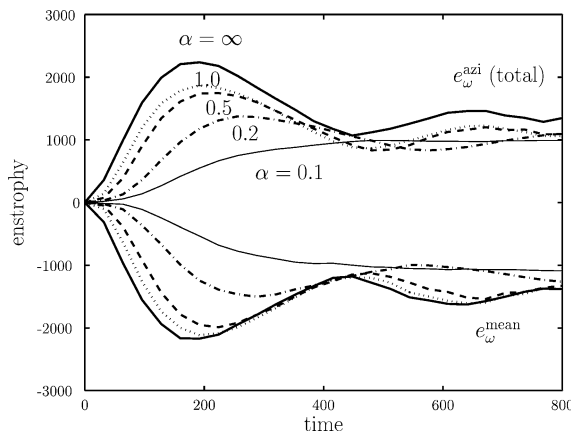


Fig. 14. Evolution of the mean and total azimuthal components of enstrophy for the time-dependent straining field $\varepsilon = \varepsilon_0 \tanh(\alpha t/20)$ for a selection of values of α . Here $\varepsilon_0 = 0.0015$ and the impulsive case corresponds to the limit $\alpha \rightarrow \infty$.

the periphery of the vortex leaving a rotating distorted core; this core winds up the stripped vorticity, but shows no tendency to relax to axisymmetry itself. This is in agreement with simulations which indicate that the sharp-edged vortices that result from stripping (and which are argued to be common in 2-d turbulence) are able to resist the processes of axisymmetrization that frequently are important for smoother vortices.

Acknowledgements

The authors thank Professor David Dritschel for providing the CASL code used for some of the calculations. We are also grateful to Professor Bill Young for sending us the preprint of [19] and to the referees for helpful comments.

References

- [1] B. Fornberg, A numerical study of 2-d turbulence, *J. Comput. Phys.* 25 (1977) 1–31.
- [2] J.C. McWilliams, The emergence of isolated coherent vortices in turbulent flow, *J. Fluid Mech.* 146 (1984) 21–43.
- [3] M.E. Brachet, M. Meneguzzi, H. Politano, P.-L. Sulem, The dynamics of freely decaying two-dimensional turbulence, *J. Fluid Mech.* 194 (1988) 333–349.
- [4] L. Ting, R. Klein, *Viscous Vortical Flows*, Lecture Notes in Physics, Vol. 374, Springer, New York, 1991.
- [5] J.F. Lingevitch, A.J. Bernoff, Distortion and evolution of a localized vortex in an irrotational flow, *Phys. Fluids* 7 (1995) 1015–1026.
- [6] K.G. Oetzel, G.K. Vallis, Strain, vortices and the enstrophy inertial range in two-dimensional turbulence, *Phys. Fluids* 9 (1997) 2991–3004.
- [7] M.T. Montgomery, R.J. Kallenbach, A theory for vortex Rossby waves and its application to spiral bands and intensity changes in hurricanes, *Quart. J. Roy. Met. Soc.* 123 (1997) 435–465.
- [8] A.P. Bassom, A.D. Gilbert, The spiral wind-up of vorticity in an inviscid planar vortex, *J. Fluid Mech.* 371 (1998) 109–140.
- [9] D.G. Dritschel, Contour dynamics and contour surgery: numerical algorithms for extended high-resolution modelling of vortex dynamics in two-dimensional, inviscid, incompressible flows, *Comput. Phys. Rep.* 10 (1989) 77–146.
- [10] D.G. Dritschel, On the persistence of non-axisymmetric vortices in inviscid two-dimensional flows, *J. Fluid Mech.* 371 (1998) 141–155.
- [11] P. Koumoutsakos, Inviscid axisymmetrization of an elliptical vortex, *J. Comput. Phys.* 138 (1997) 821–857.
- [12] L.F. Rossi, J.F. Lingevitch, A.J. Bernoff, Quasi-steady monopole and dipole attractors for relaxing vortices, *Phys. Fluids* 9 (1997) 2329–2338.
- [13] A.J. Bernoff, J.F. Lingevitch, Rapid relaxation of an axisymmetric vortex, *Phys. Fluids* 6 (1994) 3717–3723.
- [14] D.A. Schechter, D.H.E. Dubin, A.C. Cass, C.F. Driscoll, I.M. Lansky, T.M. O’Neil, Inviscid damping of asymmetries on a 2-d vortex, *Phys. Fluids* 12 (2000) 2397–2412.
- [15] S.G. Llewellyn Smith, The influence of circulation on the stability of vortices to mode-one disturbances, *Proc. Roy. Soc. London A* 451 (1995) 747–755.
- [16] R.A. Smith, M.N. Rosenbluth, Algebraic instability of hollow electron columns and cylindrical vortices, *Phys. Rev. Lett.* 64 (1990) 649–652.
- [17] R.J. Briggs, J.D. Daugherty, R.H. Levy, Role of Landau damping in crossed-field electron beams and inviscid shear flow, *Phys. Fluids* 13 (1970) 421–432.
- [18] S. Le Dizès, Non-axisymmetric vortices in two-dimensional flows, *J. Fluid Mech.* 406 (2000) 175–198.
- [19] N.J. Balmforth, S.G. Llewellyn Smith, W.R. Young, Disturbing vortices, *J. Fluid Mech.* 426 (2001) 95–133.
- [20] A.P. Bassom, A.D. Gilbert, The spiral wind-up and dissipation of vorticity and a passive scalar in a strained planar vortex, *J. Fluid Mech.* 398 (1999) 245–270.
- [21] T.S. Lundgren, Strained spiral vortex model for turbulent fine structure, *Phys. Fluids* 25 (1982) 2193–2203.
- [22] D.W. Moore, P.G. Saffman, Structure of a line vortex in an imposed strain, in: J.H. Olsen, A. Goldburg, M. Rogers (Eds.), *Aircraft Wake Turbulence and its Detection*, Plenum Press, 1971, pp. 339–354.
- [23] S. Kida, Motion of an elliptic vortex in a uniform shear flow, *J. Phys. Soc. Japan* 50 (1981) 3517–3520.
- [24] B. Legras, D.G. Dritschel, Vortex stripping and the generation of high vorticity gradients in two-dimensional flows, *Appl. Sci. Res.* 51 (1993) 445–455.
- [25] H.B. Keller, A new difference scheme for parabolic problems, in: B. Hubbard (Ed.), *Numerical Solutions of Partial Differential Equations*, Vol. 2, Academic Press, 1971, pp. 327–350.
- [26] C. Macaskill, B.M. Bewick, The use of hyperviscosity in simulations of geophysical fluid flows, in: *Proc. of the 12th Australian Fluid Mechanics Conference*, Sydney, Australia, 1995, pp. 415–418.
- [27] D.G. Dritschel, M.H.P. Ambaum, A contour-advection semi-Lagrangian algorithm for the simulation of fine-scale conservative fields, *Quart. J. Roy. Met. Soc.* 123 (1997) 1097–1130.
- [28] B. Legras, D.G. Dritschel, P. Caillol, The erosion of a distributed two-dimensional vortex in a background straining flow, *J. Fluid Mech.* 441 (2001) 369–398.
- [29] J. Jiménez, H.K. Moffatt, C. Vasco, The structure of the vortices in freely decaying turbulence, *J. Fluid Mech.* 313 (1996) 209–222.